Latest Advances of Model Predictive Control in Electrical Drives—Part II: Applications and Benchmarking With Classical Control Methods

Jose Rodriguez, *Life Fellow, IEEE*, Cristian Garcia, *Member, IEEE*, Andres Mora, *Member, IEEE*, S. Alireza Davari, *Senior Member, IEEE*, Jorge Rodas, *Senior Member, IEEE*, Diego Fernando Valencia, *Member, IEEE*, Mahmoud Elmorshedy, *Member, IEEE*, Fengxiang Wang, *Senior Member, IEEE*, Kunkun Zuo, Luca Tarisciotti, *Member, IEEE*, Freddy Flores-Bahamonde, *Member, IEEE*, Wei Xu, *Senior Member, IEEE*, Zhenbin Zhang, *Senior Member, IEEE*, Yongchang Zhang, *Senior Member, IEEE*, Margarita Norambuena, *Member, IEEE*, Ali Emadi, *Fellow, IEEE*, Tobias Geyer, *Senior Member, IEEE*, Ralph Kennel, *Senior Member, IEEE*, Tomislav Dragicevic, *Senior Member, IEEE*, Davood Arab Khaburi, Zhen Zhang, *Senior Member, IEEE*, Mohamed Abdelrahem, *Senior Member, IEEE*, and Nenad Mijatovic, *Senior Member, IEEE*

***Abstract*—This article presents the application of model predictive control (MPC) in high-performance drives. A wide variety of machines have been considered: Induction machines, synchronous machines, linear motors, switched reluctance motors, and multiphase machines. The control of these machines has been done by introducing minor and easy-to-understand modifications to the basic predictive control concept, showing the high flexibility and simplicity of the strategy. The second part of the article is dedicated to the performance comparison of MPC with classical control techniques such as field-oriented control and direct torque control. The comparison considers the dynamic behavior of the drive and steady-state performance metrics, such as inverter losses, current distortion in the motor, and acoustic noise. The main conclusion is that MPC is very competitive concerning classic control methods by reducing the inverter losses and the current distortion with comparable acoustic noise.**

Manuscript received March 27, 2021; revised July 28, 2021; accepted September 24, 2021. Date of publication October 20, 2021; date of current version January 19, 2022. This work was supported in part by ANID through projects Fondecyt under Grants 11180235, 1210208, 11190852, and FB0008, in part by the Anillo Project ACT192013, and in part by SERC Chile under Grant CONICYT/FONDAP/15110019, in part by the National Natural Science Funds of China under Grant 51877207, and in part by the Australian Government through the Australian Research Council (Discovery Project No. DP210101382). Recommended for publication by Associate Editor Lakshmi L. V. Iyer. *(Corresponding author: Cristian Garcia.)*

Jose Rodriguez, Luca Tarisciotti, and Freddy Flores-Bahamonde are with the Department of Engineering Sciences, Universidad Andres Bello, Santiago 30332, Chile (e-mail: jose.rodriguez@unab.cl; luca.tarisciotti@unab.cl; freddy.flores@unab.cl).

Cristian Garcia is with the Department of Electrical Engineering, Universidad de Talca, Curico 3340000, Chile (e-mail: cgarciap7@gmail.com).

Andres Mora and Margarita Norambuena are with the Department of Electrical Engineering, Universidad Tecnica Federico Santa Maria, Valparaiso 30332, Chile (e-mail: a.mora@ieee.org; margarita.norambuena@usm.cl).

S. Alireza Davari is with the Faculty of Electrical Engineering, Shahid Rajaee Teacher Training University, Tehran 16788 15811, Iran (e-mail: ali13davari@yahoo.com).

Jorge Rodas is with the Laboratory of Power and Control Systems, Facultad de Ingeniería, Universidad Nacional de Asunción, San Lorenzo 2160, Paraguay (e-mail: jrodas@ing.una.py).

Diego Fernando Valencia and Ali Emadi are with McMaster Automotive Resource Centre (MARC), McMaster University, Hamilton, ON L8P 0A6, Canada (e-mail: valend1@mcmaster.ca; emadi@mcmaster.ca).

Mahmoud Elmorshedy is with the Department of Electrical Power and Machines Engineering, Faculty of Engineering, Tanta University, Tanta 31521, Egypt (e-mail: mahmoud.elmorshedy@f-eng.tanta.edu.eg).

Fengxiang Wang is with the Quanzhou Institute of Equipment Manufacturing, Haixi Institutes, Chinese Academy of Sciences, Beijing 362200, China (e-mail: fengxiang.wang@fjirsm.ac.cn).

Kunkun Zuo is with the Quanzhou Institute of Equipment Manufacturing, Haixi Institutes, Chinese Academy of Sciences, Beijing 362200, China, and also with the Institute for Electrical Drive Systems and Power Electronics, Technical University of Munich (TUM), 80333 Munich, Germany (e-mail: zuokunkun17@mails.ucas.ac.cn).

Ralph Kennel is with the Institute for Electrical Drive Systems and Power Electronics, Technical University of Munich (TUM), 80333 Munich, Germany (e-mail: ralph.kennel@tum.de).

Wei Xu is with the State Key Laboratory of Advanced Electromagnetic Engineering and Technology, School of Electrical and Electronic Engineering, Huazhong University of Science and Technology, Wuhan 430074, China (e-mail: weixu@hust.edu.cn).

Zhenbin Zhang is with the School of Electrical Engineering, Shandong University, Jinan 250061, China (e-mail: zbz@sdu.edu.cn).

Yongchang Zhang is with the School of Electrical and Electronic Engineering, North China Electric Power University, Beijing 102206, China (e-mail: yozhang@ieee.org).

Tobias Geyer is with ABB System Drives, 5300 Turgi, Switzerland (e-mail: t.geyer@ieee.org).

Tomislav Dragicevic and Nenad Mijatovic are with the Department of Electrical Engineering, Technical University of Denmark, 2800 Lyngby, Denmark (e-mail: tomdr@elektro.dtu.dk; nm@elektro.dtu.dk).

Davood Arab Khaburi is with the Department of Electrical Engineering, Iran University of Science and Technology, Tehran 1311416846, Iran (e-mail: khaburi@iust.ac.ir).

Zhen Zhang is with the School of Electrical and Information Engineering, Tianjin University, Tianjin 300072, China (e-mail: zhangz@tju.edu.cn).

Mohamed Abdelrahem is with the Institute for Electrical Drive Systems and Power Electronics, Technical University of Munich (TUM), 80333 Munich, Germany, and also with Electrical Engineering Department, Faculty of Engineering, Assiut University, Assiut 71516, Egypt (e-mail: mohamed.abdelrahem@tum.de).

Color versions of one or more figures in this article are available at https://doi.org/10.1109/TPEL.2021.3121589.

Digital Object Identifier 10.1109/TPEL.2021.3121589

***Index Terms*—Electric machine, predictive control, variable speed drives.**

I. Introduction

With the advances of electromobility, the control of electrical machines, a traditional research area, is now more active than ever [1]–[3]. Applications of controlled electrical motors in cars, trucks, buses, trains, scooters, and bicycles are intensively investigated [4]–[11]. Different types of motors are being studied for these applications: Induction machines (IM), permanent magnet synchronous machines (PMSM), and switched reluctance machines (SRM) to mention a few [5], [12]–[14].

Today, the dominant strategy for the control of electrical motors in electromobility is field oriented control (FOC). This technique was invented 50 years ago at a time where microprocessors were not available [15], [16]. Using microprocessors this technique constantly has been improved and today is the standard for high performance drives.

The tremendous calculation power of modern microprocessors available today has motivated the investigation of different control techniques for high performance drives, with model predictive control (MPC) being one of them. MPC has emerged as a very attractive alternative for drives applications, because it adapts in a very natural way the discrete nature of the controller (the microprocessor) to the load, which is a system with a finite number of switching states generated by the inverter. Using MPC it is not necessary to linearize the equations of the machine, to design linear controllers and to use PWM [17]–[21]. Several works have been published, related to the use of MPC in electrical drives [22]–[27].

This article presents a review of recent and relevant MPC strategies applied to different types of machines: Induction motors, synchronous motors, switched reluctance motors, multiphase motors, and linear motors. This article shows how MPC is adapted to fulfill the particular restrictions presented by each electric machine type.

Aiming to be accepted by the industry, MPC techniques must demonstrate superior performance compared to existing high-performance strategies: FOC and direct torque control (DTC). For doing so, the second part of this review article is dedicated to assessing the performance of these control techniques. The main comparison criteria evaluate the dynamic behavior of electromagnetic torque. The assessment also considers steady-state performance metrics such as switching losses in the inverter, the ripple in the motor current, and the motor's acoustic noise, which is relevant for car applications.

The rest of this article is organized as follows. Section II presents a short review of the main MPC strategies. Sections III–V present the main features related to the application of MPC in switched reluctance, linear induction, and multiphase machines, respectively. Section VI compares a model predictive torque control (MPTC) strategy based on finite control set MPC (FCS-MPC) with the two most important high-performance control strategies used in industry, namely: FOC and DTC. The comparison evaluates the steady-state and dynamic performance. Section VII compares the technique called model predictive pulse pattern control (MP^{3}C), [28]–[34] with standard control techniques, applied in a high power (>1 MW) drive, using a three-level neutral point clamped (NPC) inverter. Section VIII compares the model predictive current control with linear current control and PWM for an electric car application, considering the losses of the inverter and acoustic noise [35]. Section IX presents the challenges and future works. Finally, Section X concludes this article.

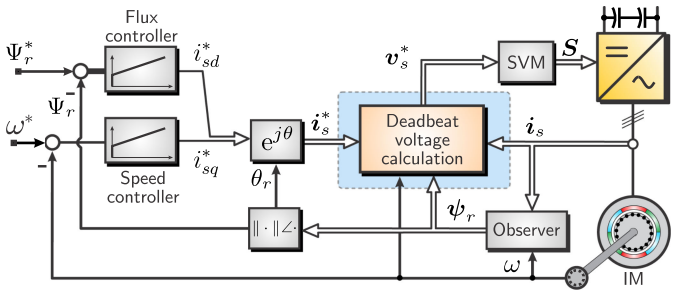

Fig. 1. Deadbeat-based FOC method.

II. Predictive Control Strategies for Drives

The predictive control method includes different subbranches, i.e., hysteresis-based control, trajectory-based control, deadbeat control, and MPC [36] [21]. The hysteresis control theory, which is also known as bang-bang control theory, was first introduced for predictive current control in [37]. The trajectory control method is based on forcing the variables of the system to track a predefined trajectory. Direct self control [38] and direct mean torque [39] are the most important methods in this category [40]. The combination of the hysteresis-based control and the trajectory-based control has become an independent family in the drive applications known as the direct toque control [41]. This method showed that the predictive control is capable of the direct control of the desired variables like the torque and the flux [40]. Except for the DTC strategy, today two successful categories of the predictive control family in drive applications are deadbeat control, and MPC. These two categories were widely investigated for the drive applications during the last decade. The MPC method has been applied by two approaches, i.e., continuous control set MPC (CCS-MPC) and FCS-MPC.

A. Deadbeat Control in Drive Applications

The idea of the deadbeat control is based on calculation and application of the voltage vector that will move the operating point of the motor exactly to the desired torque and the flux [42]. The deadbeat method has been applied to drive applications because of the capability of a very fast dynamic response [43] and the accurate steady state response [42]. Fig. 1 shows a typical block diagram of the deadbeat control method for motor drives in field coordinates. The following equation shows the voltage reference calculation in deadbeat control of the induction motor

[44]:

$$\boldsymbol{v}_s^* = \frac{\sigma L_s}{T_s}\left(\boldsymbol{i}_s^* - \boldsymbol{i}_s^k\right) + R_\sigma \boldsymbol{i}_s^k + \frac{k_r}{\tau_r}\left(j\omega\tau_r - 1\right)\boldsymbol{\psi}_r^k \quad (1)$$

where $\tau_r = \frac{L_r}{R_r}$, $k_r = \frac{L_m}{L_r}$, $R_\sigma = R_s + k_r^2 R_r$, $\sigma = 1 - \frac{L_m^2}{L_s L_r}$, and T_s is the sampling period.

Despite the mentioned advantages of this technique, it shows a high sensitivity to different kinds of disturbances in practice. Most of the studies about the deadbeat method during the last decade are dedicated to robustness improvement. The research on this issue can be categorized as follows:

1) disturbance estimation and cancellation;
2) controller bandwidth tuning;
3) online parameter identification;
4) prediction model robustness improvement.

The disturbance estimators are used to estimate the general errors produced by the system's disturbances [45]. The estimated disturbance should be subtracted by the control law, which is the stator voltage reference. In [46], an ultralocal model is used to observe the system's disturbance. A combination of disturbance and load observers is proposed as the parallel observer in [47].

Another technique to increase the deadbeat method's robustness to reduce the controller bandwidth was introduced in [43]. The bandwidth reduction of the controller is performed by dividing the error by two [47]. Through this technique, the tolerance of the parameters can be increased up to 200% while decreasing the deadbeat controlled system's dynamic performance.

The adaptive online parameter identification has been widely utilized to improve the robustness of the deadbeat method [42]. A model reference adaptive system (MRAS) observer is used in [48] to adapt the speed and stator resistance simultaneously. The results of this article showed that a 150% uncertainty of the stator resistance is tolerated. However, the drift error is a common problem among MRAS-based observers. In [42], the estimation is performed one step ahead to reduce the drift error.

The closed-loop Luenberger prediction model has been introduced as the robust prediction model [49]. The feedback gains are calculated based on the H_∞ robust design. Although this method increases the robustness, it is proved that the method is not robust at near-zero speed region. In [50] and [51], an integrator is used in the control loop to reduce the sensitivity and modify the dynamic response of the system.

Overall, the deadbeat control method is considered the faster control method in the predictive control family. Consequently, the sensitivity to parameters mismatch and estimation of disturbances are the main issues to overcome about this control method to achieve a high-performance motor drive controller.

B. Continuous Control Set MPC

This control strategy was first introduced as the generalized predictive control [52] and it is considered the basic form of MPC. As shown in Fig. 2, this control method employs carrier-based PWM such as sinusoidal PWM or space vector modulation (SVM) and it is also referred to as indirect MPC [21].

This control method computes the voltage reference by minimizing a given cost function, representing the tracking error

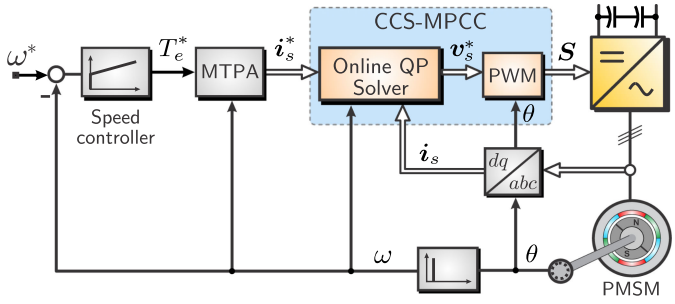

Fig. 2. CCS-MPC-based MPTC for PMSMs.

of the controlled variables. The cost function for current control considering a prediction horizon of one step is defined as follows [53]

$$g = \left(i_{sd}^* - i_{sd}^{k+1}\right)^2 + \left(i_{sq}^* - i_{sq}^{k+1}\right)^2. \quad (2)$$

Suppose both the constraints related to the feasibility region in which the voltage vector belongs (input constraints) and the current limits (state constraints) are not considered. In that case, an unconstrained quadratic programming (QP) is established, and the voltage vector can be easily obtained by solving $\nabla g = 0$. For instance, if a surface-mount PMSM is utilized, the optimized voltage variables v_{sd}^k and v_{sq}^k are

$$v_{sd}^k = \frac{L_s}{T_s}(i_{sd}^* - i_{sd}^k) + R_s i_{sd}^k - L_s \omega^k i_{sq}^k \quad (3a)$$

$$v_{sq}^k = \frac{L_s}{T_s}(i_{sq}^* - i_{sq}^k) + R_s i_{sq}^k + L_s \omega^k i_{sd}^k + \omega^k \psi_{\mathrm{pm}}. \quad (3b)$$

The studies in [53]–[55] show that the CCS-MPC results in a low ripple for the torque and the current of the machine. Also, the computational burden of this control method is low. However, as shown in (3), the performance of the controller would be deteriorated by the parameter variations (including stator resistance, stator inductance, and permanent magnet flux linkage) and nonlinearity. Thus, the sensitivity of the method is high, similar to the deadbeat control strategy.

To overcome this issue, many approaches have been proposed in the literature. For instance, as indicated in [21], the robustness of the Indirect MPC is improved by penalizing the control effort[1] in the cost function allowing for less aggressive control actions. In [53], a disturbance observer is applied to reduce the sensitivity of the method. Besides, the rotor position is eliminated from the prediction model in [55] to increase the robustness of the sensorless motor drive.

Furthermore, when input and/or state constraints are considered for the MPC formulation [21], then either efficient QP solvers can be employed (e.g., interior-point, active-set methods [56]), or the unconstrained solution can be projected onto the feasible set. In [57], a CCS-MPC strategy with input and state constraints was introduced for MPTC in PMSMs, in which

[1]In CCS-MPC, the control effort stands for change in the voltage vector or change in the modulation index. In the context of FCS-MPC, the control effort concept refers to the switching effort and penalizes the number of commutations of the power semiconductors.

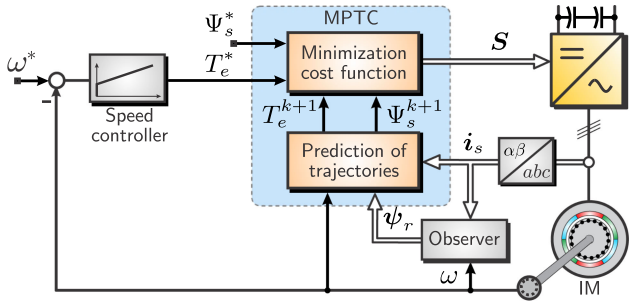

Fig. 3. FCS-MPC-based MPDT for IMs.

an active-set algorithm to solve efficiently the associated QP problem is implemented in a low-cost control platform.

C. Finite Control Set MPC

The distinguishing point of this MPC approach is the consideration of the finite nature of the power converter. Considering this feature, the FCS-MPC predicts the behavior of the variable to be controlled for a set of admissible switching positions. The cost function should be examined for all feasible voltage vectors, and the optimum switching state is the one minimizing the cost function. For instance, if a traditional two-level inverter is utilized and a prediction horizon of one step is considered, the cost function should be evaluated for the set of possible voltage vectors [58]–[60].

The block diagram of the FCS-MPC method applied for MPTC is illustrated in Fig. 3. As indicated above, the stator flux and electromagnetic torque of the IM can be predicted by using [61]

$$\boldsymbol{\psi}_s^{k+1} = \sigma L_s \boldsymbol{i}_s^{k+1} + k_r \boldsymbol{\psi}_r^{k+1} \tag{4a}$$

$$T_e^{k+1} = \frac{3}{2} \boldsymbol{\psi}_s^{k+1} \times \boldsymbol{i}_s^{k+1}. \tag{4b}$$

In (4), the future trajectories for the stator current $\boldsymbol{i}_s^{k+1}$ and rotor flux $\boldsymbol{\psi}_r^{k+1}$ are obtained from the following discrete-time model:

$$\begin{bmatrix} \boldsymbol{i}_s^{k+1} \\ \boldsymbol{\psi}_r^{k+1} \end{bmatrix} = \begin{bmatrix} 1-\frac{T_s R_\sigma}{\sigma L_s} & \frac{T_s k_r}{\sigma L_s}\left(\frac{1}{\tau_r} - j\omega^k\right) \\ \frac{T_s L_m}{\tau_r} & 1-T_s\left(\frac{1}{\tau_r} - j\omega^k\right) \end{bmatrix} \begin{bmatrix} \boldsymbol{i}_s^k \\ \boldsymbol{\psi}_r^k \end{bmatrix} + \begin{bmatrix} \frac{T_s}{\sigma L_s} \\ 0 \end{bmatrix} \boldsymbol{v}_s^k. \tag{5}$$

The cost function for controlling the torque and stator flux magnitude is

$$g_j = \left(T_e^* - T_{ej}^{k+1}\right)^2 + \lambda_\Psi \left(\Psi_s^* - \Psi_{sj}^{k+1}\right)^2. \tag{6}$$

Consequently, the cost function (6) should be computed for all possible voltage vectors according to the FCS-MPC working principle, where λ_Ψ is the flux weighting factor. Then, the inverter applies the voltage vector that minimizes the cost function. This process is repeated each control interval T_s.

The advantages of the FCS-MPC can be summarized as follows [60]–[64].

1) It is straightforward to include nonlinearities, constraints, and variables of different nature in the optimization problem.
2) There is no need for a modulator which is useful when a multilevel or a matrix converter is applied.
3) The dynamic performance of the control method is faster than the one obtained with FOC.

Despite the mentioned advantages, there are some drawbacks with the FCS-MPC method. The first problem is the weighting factor in the cost function which is the common problem of all cost function-based MPC methods [65]. Generally, four techniques have been applied for this problem;

1) finding the optimum weighting factors [66];
2) simplified FCS-MPC [67];
3) decision-making-based methods [68];
4) sequential FCS-MPC [22].

The second drawback of the FCS-MPC is the high ripple for the torque and the current. A promising solution to mitigate these issues is the so-called modulated MPC strategy introduced in [69] and [70] for PMSMs. Similar to the modulated MPC, a control strategy that manipulates the switching states and their application times aiming to control the stator flux trajectory is proposed in [71] to improve the overall performance of IM-based drives.

The last problem of FCS-MPC is the high computational burden when it is adapted for multilevel converter applications. Voltage vector elimination has been utilized in [72] aiming to reduce the number of possible vectors that should be calculated.

III. Application of FCS-MPC in SRM

SRMs, magnet-free, and double salient pole structure offer a simpler construction and robust high-speed and high-temperature operation [73], making them interesting for reliable fault-tolerant operation [74]. These features have found a suitable position in applications such as vacuum cleaners, jack hammers, compressors, and electric vehicle systems [75], [76]. Although SRMs are candidates for high-performance and safety–critical systems such as automotive traction or aerospace [77], [78], in practice, they have not seen such scenarios due to their inherent torque ripple and acoustic noise [79].

Several design considerations have been proposed and comprehensively reviewed in [80]–[82]. However, torque control is not as straightforward as it is in conventional ac drives. The highly nonlinear torque-current-position relation requires the definition of torque sharing rules that are mapped as phase reference currents through lookup tables [83], in a similar way as FOC. Some of these rules include torque sharing functions (TSFs) [84] or radial force shaping (RFS) algorithms [85]. Nevertheless, the current tracking is a challenging task in such a nonlinear machine. This high complexity has become an interesting target for MPC to handle.

1) MPC of SRM Drives: There are two alternative implementations of MPC in SRM, as shown in Fig. 4. The first one, in Fig. 4(a), emulates the FOC obtaining reference currents from precalculated lookup tables. A model predictive current control (MPCC) algorithm tracks the phase currents based on the discrete machine flux equation as [86]

$$\psi_j^{k+1} = \psi_j^k(i_j^k, \theta_j) + T_s(v_j^k - R_j i_j^k) \tag{7}$$

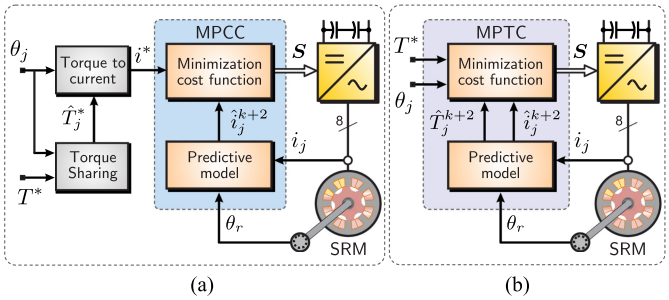

Fig. 4. Block diagram for control algorithms in SRM drives. (a) Current reference generated with offline torque sharing technique and MPCC for phase current tracking. (b) MPTC.

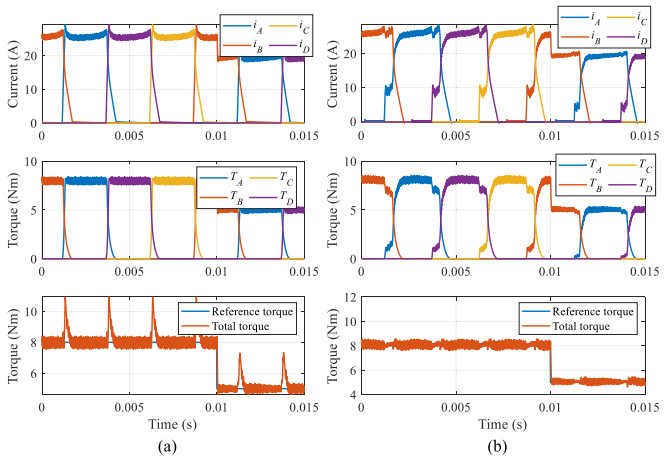

Fig. 5. Results for torque tracking at 1000 r/min of a four-phase 8/6 SRM using (a) TSF and MPCC, and (b) MPTC.

where v_j, i_j, R_j, L_j, and ψ_j are the voltage, current, resistance, and flux linkage of the phase j, respectively. Notice that the dependence of the flux linkage on both the current and electrical angle θ_j is highly nonlinear; therefore, the predictive model usually relies either on approximated analytical equations or static maps [87]. In the latest, ψ_j^k is obtained from the static characteristics $\psi(i,\theta)$ as a lookup table. The predicted ψ_j^{k+1} is used to obtain i_j^{k+1} using a second lookup table $i(\psi,\theta)$. In practice, this prediction uses on ψ_j^{k+2} for delay compensation. Alternatively, Fig. 4(b) uses an MPTC approach, which generates a switching pattern with the comparison of the reference torque and the predicted torque from the predictive model [88]. The main advantage is the online definition of torque sharing laws. The torque T_{ej}^{k+1} is predicted from the phase torque T_{ej}^{k+1} and i_j^{k+1} as

$$T_e^{k+1} = \sum_{j=1}^{m} T_{ej}^{k+1}\left(i_j^{k+1}, \theta_j^{k+1}\right). \tag{8}$$

2) Cost Functions: The current tracking can be defined with (9a) [89]. As the SRMs commonly use asymmetric converters, there are three possible switching states per phase. For a four-phase SRM it means $3^4 = 81$ possible combinations. Assuming no more than two phases simultaneously active, it is reduced to 9 possible states [86]. For the MPTC approach, (9b) can be adopted [88], [90]. It is common to include a term to penalize the phase currents to obtain the reference torque with the minimum conduction losses [91]. The cost functions in (9) evaluate the possible switching states to obtain the S_{opt}^{k+2} that minimizes the error. Fig. 5 shows the phase currents, phase torque, and total torque for the algorithms shown in Fig. 4. MPCC guarantees proper current regulations with minimum ripple, but the algorithm, in this case TSF, fails to reduce torque ripple requiring additional improvement. MPTC, contrarily, provides a smooth torque sharing with more diverse current waveforms, thus evidencing the flexibility of MPCC

$$g_i = \left(i^* - {i_j}^{k+2}\right)^2 \tag{9a}$$

$$g_{T_e} = \left(T_e^* - T_{ej}^{k+2}\right)^2 + \sigma_i \sum i_j. \tag{9b}$$

3) Particular Considerations and Constrains: SRM control usually rely on finite element analysis models to obtain the static maps, which possibly makes the parameter variations considerable. Solutions have been proposed like online parameter estimation to compensate for variations in the phase inductance and filtering techniques for measurement inaccuracies [92]. MPC for SRM is still at an early stage, and further work on secondary objectives such as acoustic noise and fault-tolerance is still required.

IV. Application of FCS-MPC in Linear Induction Machine

Linear IM (LIMs) have many applications such as reciprocating compressor, packing materials handling, and also it is used in subway systems in various countries such as the USA, Japan, and China [93]–[95]. Despite comprehensive research of MPC for conventional rotating machines presented in [93] and [96], few works have focused on MPC for LIM applications. Different MPC strategies have been presented for LIM applications [96]–[104]. Some of these strategies have focused on the reduction of thrust and primary flux-linkage ripples, the decreasing distortion of the primary current, achieving the maximum thrust per ampere (MThPA), and eliminating the weighting factor from the cost function.

In [97], both running and safety operation for the LIM have been improved by applying multistep MPC (MMPC). Meanwhile, the development of two or three voltage vectors has been proposed in [98] and [99] so as to reduce the current ripples. In [98], the armature current has been limited within a safe region by inserting a penalty overcurrent factor in the designed cost function. Moreover, an improved deadbeat control with an iterative algorithm is proposed in [99] to solve the problem of current and voltage constraints in the traditional DBC. In addition, the deadbeat control has been improved by producing the maximum thrust in the whole working condition [100]. Further, the FCS-MPC is improved by adding the MThPA criteria with different condition such as presented in [101]–[103]. Finally, some researchers have developed the MPC without weighting factor to reduce the time consumed, such as [96] and [104].

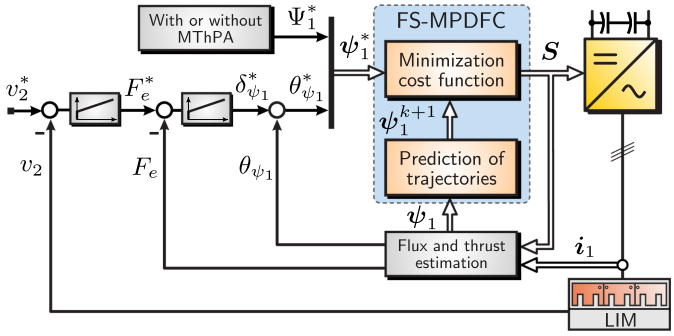

Fig. 6. Proposed MThPA based the FS-MPDFC for LIM drive system.

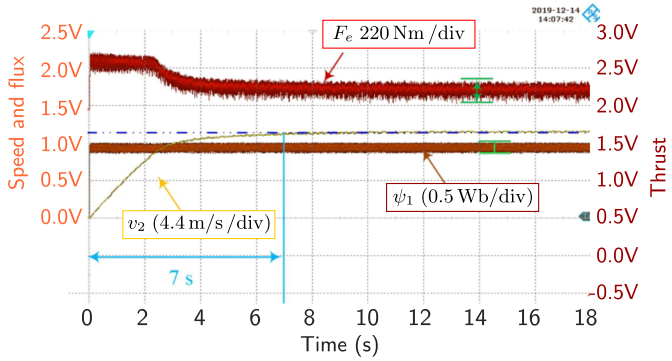

Fig. 7. Responses of thrust, primary flux-linkage, and linear speed for LIM based on FS-MPDFC.

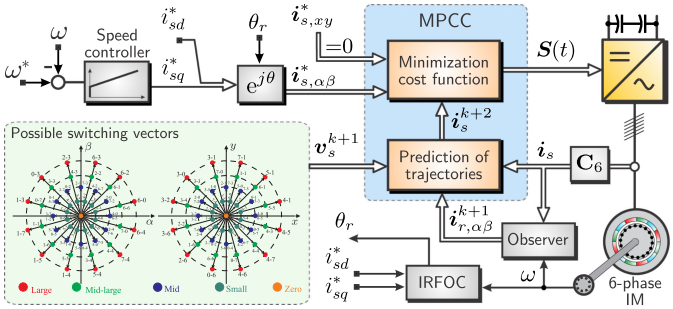

Fig. 8. Voltage space vectors and 64 switching states in $\alpha-\beta$ and $x-y$ planes and MPCC scheme for a six-phase IM.

In order to completely eliminate the weighting factors, reduce the calculation process, and improve the performance of the LIM drive system, a new cost function is proposed in [101]. The new cost function is based only on the primary flux-linkage error. Extra improvement can be accomplished with the proposed control approach by achieving MThPA criterion. This method is called finite-set model predictive direct flux control (FS-MPDFC).

Based on the dynamic model of the LIM, the error between the reference thrust and the actual thrust $\Delta F_e = F_e^* - F_e$ can be expressed by [103]

$$\Delta F_e = \frac{3}{2}\frac{\pi}{\tau}\frac{1}{\tau_l \sigma}\|\boldsymbol{\psi}_1\|\|\boldsymbol{\psi}_2\|\big(\sin(\theta_{12}+\delta_{\boldsymbol{\psi}1})-\sin(\theta_{12})\big) \quad (10)$$

where θ_{12} is the angle between the primary and secondary flux-linkages. Notice that, from (10), the relation between the thrust error and the incremental deviation of the thrust angle, $\delta_{\boldsymbol{\psi}1}$ is nonlinear. Therefore, a PI controller is used to generate the incremental variation of the thrust angle. Hence, the reference primary flux-linkage can be calculated by

$$\psi_{1\alpha}^* = \|\boldsymbol{\psi}_1^*\|\cos(\theta_{\Psi_1}+\delta_{\boldsymbol{\psi}_1}) \quad (11)$$

$$\psi_{1\beta}^* = \|\boldsymbol{\psi}_1^*\|\sin(\theta_{\Psi_1}+\delta_{\boldsymbol{\psi}_1}) \quad (12)$$

where $|\boldsymbol{\psi}_1^*|$ is the amplitude of reference primary flux-linkage, and $\theta_{\Psi 1}$ the angle of the estimated primary flux linkage. In order to guarantee the maximal thrust, the reference primary flux-linkage $|\boldsymbol{\psi}_1^*|$ can be calculated based on [101].

The proposed cost function depends only upon $\boldsymbol{\psi}_{\alpha\beta}$ reference and predicted components as expressed by

$$g = \left(\psi_{1\alpha}^* - \psi_{1\alpha,i}\right)^2 + \left(\psi_{1\beta}^* - \psi_{1\beta,i}\right)^2. \quad (13)$$

The block diagram of the proposed FS-MPDFC strategy is shown in Fig. 6. The final expression of the predicted primary flux-linkage can be written as

$$\psi_{1\alpha,i}(k+1) = \psi_{1\alpha}(k) + T_s(u_{1\alpha,i}(k) - R_1 i_{1\alpha}(k)) \quad (14)$$

$$\psi_{1\beta,i}(k+1) = \psi_{1\beta}(k) + T_s(u_{1\beta,i}(k) - R_1 i_{1\beta}(k)). \quad (15)$$

The proposed FS-MPDFC is tested under the thrust load of 100 N, linear speed of 6 m/s and sample time of $2\cdot 10^{-4}$s. The responses of electromagnetic thrust, primary flux linkage, and linear speed are shown in Fig. 7. It is observed that the FS-MPDFC can achieve faster response with lower thrust ripple compared to the other FS-MPDTC method mentioned in [101].

V. Application of FCS-MPC in Multiphase Machine

Multiphase systems are those that have more than three phases ($n = 5, 6, 7, 9, 12, \ldots$) and could be of either induction or synchronous type. The possibility to split the power into more phases and its inherent fault-tolerance operation with no extra hardware are the main advantages compared with traditional three-phase systems [105]. For that reasons, multiphase systems are considered ideal for fault-tolerant and high-power applications such as electric propulsion and traction (i.e., ships and electric vehicles) and generation systems (i.e., offshore wind energy systems) [106]. Nevertheless, the additional degrees of freedom (typically named $x-y$ planes) that exist in multiphase systems also make them a good alternative for various nontraditional purposes such as battery chargers for electric vehicles or multimotor systems fed by a single power converter [107].

The application of new control techniques for multiphase systems has been undoubtedly one of the main research topics that has caught the attention of the MPC community. Therefore, much effort has been directed over the last decade to improve the performance of traditional control schemes by using MPC-based controllers. The application of FCS-MPC as a MPCC for multiphase machines is presented below, taking a six-phase IM as an illustrative example.

A. Standard MPCC of Multiphase Machines

Fig. 8 shows the control structure of a six-phase IM variable speed drive using the standard indirect rotor FOC (IRFOC)

technique, where the inner current control loop is implemented with the standard MPCC. Then, the stator current reference in the $\alpha-\beta$ plane ($\boldsymbol{i}^*_{s,\alpha\beta}$) is generated from the outer speed control loop and from the d-axis current reference (i^*_{sd}). The MPCC uses the following discrete-time model of the system to predict the future values of the six-phase IM's currents $\boldsymbol{i}_m = \left[\boldsymbol{i}^T_{s,\alpha\beta}\, \boldsymbol{i}^T_{s,xy}\, \boldsymbol{i}^T_{r,\alpha\beta}\right]^T$:

$$\boldsymbol{i}^{k+1}_m = \boldsymbol{A}^k \boldsymbol{i}^k_m + \boldsymbol{B}\boldsymbol{v}^k_s \tag{16}$$

where $\boldsymbol{i}_{s,\alpha\beta} = \left[i_{s\alpha}\, i_{s\beta}\right]^T$ and $\boldsymbol{i}_{s,xy} = \left[i_{sx}\, i_{sy}\right]^T$ denote the stator current in the $\alpha-\beta$ and $x-y$ planes, respectively. The rotor current is defined accordingly $\boldsymbol{i}_{r,\alpha\beta} = \left[i_{r\alpha}\, i_{r\beta}\right]^T$. Matrices $\boldsymbol{A}^k$ and $\boldsymbol{B}$ depend on the six-phase IM parameters and the present value of both, the rotor speed ω^k and the sampling time T_s. The input stator voltages are denoted by $\boldsymbol{v}_s = \left[\boldsymbol{v}^T_{s,\alpha\beta}\, \boldsymbol{v}^T_{s,xy}\right]^T$. To provide delay compensation, a two-step ahead prediction of the stator currents $\boldsymbol{i}_s = \left[\boldsymbol{i}^T_{s,\alpha\beta}\, \boldsymbol{i}^T_{s,xy}\right]^T$ is typically performed. To this end, it is necessary to estimate and predict the unmeasurable rotor currents at instant $k+1$ [108], [109].

The cost function (17) is used to define the desired behavior, i.e., the stator current tracking. For a six-phase IM, the cost function is evaluated 49 times, and then, the voltage source inverter (VSI) switching state (S^{k+2}_{opt}) for the stator voltage vector that minimizes the cost function is selected and applied to the six-phase IM by means of the VSI during the next sample time

$$g = \left\|\boldsymbol{i}^{*k+2}_{s\alpha\beta} - \boldsymbol{i}^{k+2}_{s\alpha\beta}\right\|^2_2 + \lambda_{xy}\left\|\boldsymbol{i}^{*k+2}_{sxy} - \boldsymbol{i}^{k+2}_{sxy}\right\|^2_2. \tag{17}$$

The tuning of the weighting factor (λ_{xy}) is a heuristic procedure providing tradeoff between the variables of interest [111]. Other examples of cost functions for multiphase machines include reduction of common-mode voltages, torque ripple minimization, and VSI switching losses [112], [113].

B. Particular Considerations and Constraints

The standard MPCC is an alternative to the inner PI current controller used in typical FOC schemes. The latter technique is one of the most used control structures for multiphase machines. Compared to the standard PI current controller, MPCC provides faster current tracking and wider current control bandwidth at the expense of a higher computational cost, worse $x-y$ current control, and higher current ripple. An open issue is the simultaneous control of primary $\alpha-\beta$ flux/torque production plane and secondary $x-y$ machine losses plane. Many variations of the standard PCC have been proposed for this problem. Fig. 9 summarizes the experimental results for some of the most recent variations of the MPCC method, namely, the MPCC with virtual vector (MPCC-VV) [114], modulated MPC (M2PC) [115], and a novel variation named N-M2PC [110]. The most recent reviews of PCC structures with different cost functions for five-phase IM and six-phase IM are available in [116] and [117], respectively.

VI. General Assessment of FCS-MPC with High Performance Control Strategies

From the theoretical point of view [118]–[120], the comparison of FOC, DTC, and MPTC (see the Fig. 2 in article part I) is summarized in Table I, including the required tuned parameters,

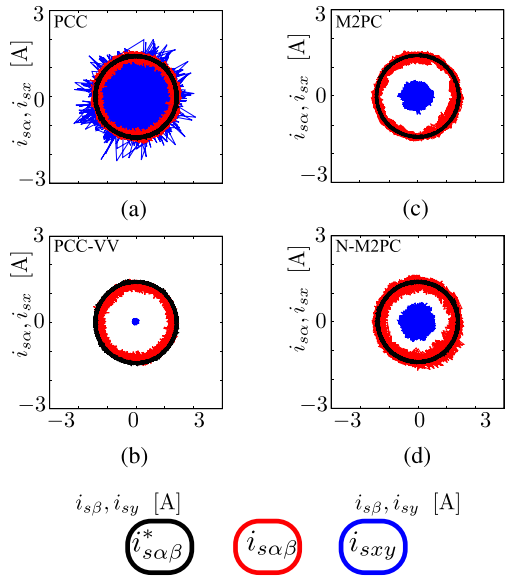

Fig. 9. Experimental stator current responses presented in [110] using (a) standard MPCC, (b) MPCC-VV, (c) M2PC, and (d) N-M2PC control methods. The same stator current references are applied for all controllers (reproduced from [110]).

TABLE I
CONTROL ALGORITHMS COMPARISON

	FOC	DTC	MPTC
Tuned Param.	6	4	3
Exter. Control	PI	PI	PI
Inner Control	2 PI	2 Hys. Contr.	Pred. Contr.
Flux Angle	Yes	Yes	No
Coordinate Transf.	Yes	No	No
PWM	Yes	No	No
Constraints inclusion	Difficult	Difficult	Easy
Control Complex.	High	High	Low
Computational Burden	8 μs	8 μs	12 μs

external loop controller, inner loop controller, system control, etc. In this section, these methods are studied comparatively by using experimental tests.

A. Evaluation Criteria

1) Switching Frequency: Unlike the FOC method, where the carrier frequency f_c of the PWM imposes the switching frequency as $f_{sw} = f_c/2$, the DTC and MPTC strategies perform variable switching frequency. Thus, to ensure a fair comparison, the goal is to establish an average switching frequency equal to the one obtained using FOC. To this end, the DTC's switching frequency is taken as a reference to adjust the sampling frequency used in the MPTC and the PWM's carrier frequency employed in the FOC.

2) Steady-State Performance: The standard deviation (SD) is used in this work to quantify the torque ripple. Besides, the current total harmonic distortion (THD) is used to compare the performance of the tested control methods.

TABLE II
PARAMETERS OF THE IM

Parameter		Value
dc-link voltage	V_{dc}	582 V
Stator resistance	R_s	2.68 Ω
Rotor resistance	R_r	2.13 Ω
Mutual inductance	L_m	275.1 mH
Stator inductance	L_s	283.4 mH
Rotor inductance	L_r	283.4 mH
Nominal Speed	ω_{nom}	2772 rpm
Nominal Torque	T_{nom}	7.5 Nm
Rotational inertia	J	0.005 kg/m^2

3) Dynamic Performance: In this article, the time for the electromagnetic torque to reach the reference is used to evaluate all control algorithms' dynamic performance.

B. Performance Evaluation

The IM test bench consists of two 2.2-kW squirrel-cage IM. The load machine is controlled by a 3.0-kW Danfoss VLT FC302 inverter to provide load torque, and the main machine is driven by a 14-kVA servostar600 inverter. The parameter of the IM are summarized in Table II. A self-made 1.4-GHz real-time computer system, Embedded PC104, is used for the control system of the inverter, with 16-kHz sampling frequency. All methods are carried out experimentally on the same test bench and using the same speed PI controller with 8-rad/s bandwidth.

To demonstrate the steady-state performance of all methods, the first comparative experiment is tested at full speed (2772 r/min) with a full load torque (7.5 N·m), as shown in Fig. 10. It should be noted that we have done a lot of experiments to tune the relevant parameters to achieve the optimal performance of each method. The measured THD of FOC, DTC, and PTC are 3.2%, 4.0%, and 3.6%, respectively. It is clear that FOC algorithm achieves the best current performance at this operating point. FOC and PTC achieve smaller torque ripples, which are 0.8 and 0.9 N·m, and the SD of torque are 0.1473 and 0.1852, respectively. DTC has slightly bigger ripples of 1.2 N·m, and the SD is 0.2227.

At the same time, when evaluating the error between the observed load reference value (7.5 N·m) and the torque fluctuation average value, only the FOC algorithm achieves a zero torque tracking error, which is due to the use of internal current PI controllers and the modulator. However, more PI parameters need to be tuned for a cascaded control structure.

Dynamic performance is one of the important indicators for evaluating various algorithms. Therefore, the torque dynamics of all methods are compared in the second test under the step-change load torque (from 0 to 7.5 N·m), as shown in Fig. 11. From this picture, we can see that FOC algorithm takes a long time (2 ms) to reach the torque reference, because the inner current loop with limited bandwidth will limit the dynamics of the outer speed loop and the use of modulator will cause a delay. On

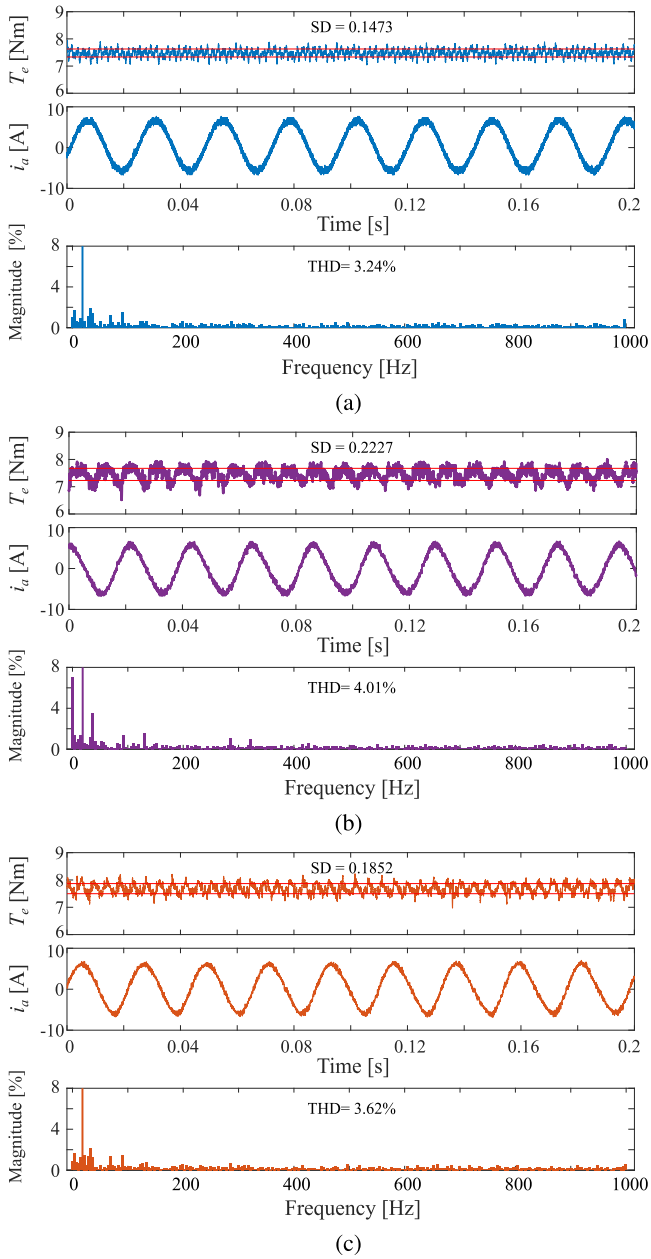

Fig. 10. Experimental results: Steady-state performance under three control algorithms. (a) FOC. (b) DTC. (c) MPTC.

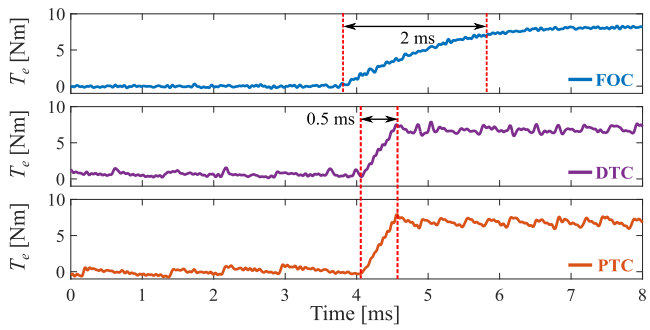

Fig. 11. Experimental results: Dynamic torque response under three control algorithms.

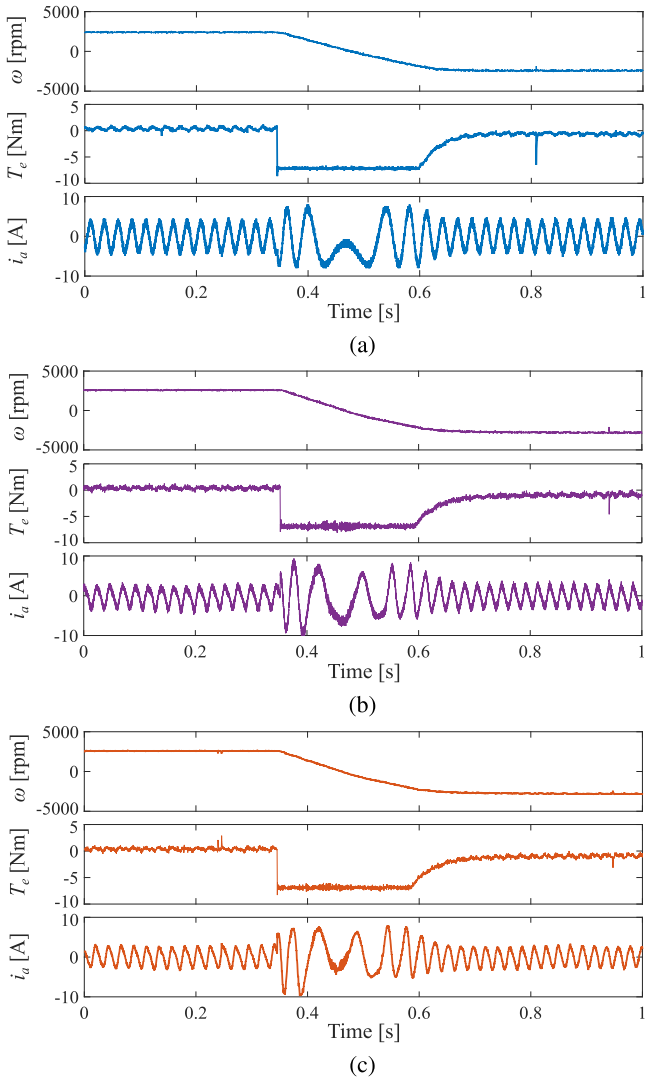

Fig. 12. Experimental results: reversal performance under three control algorithms. (a) FOC. (b) DTC. (c) MPTC.

the contrary, DTC and MPTC exhibit a shorter dynamic process (0.5 ms) because they have theoretically unlimited bandwidth. However, the primary disadvantage of the direct control method is that the selected voltage vector will be kept throughout the control interval, which possibly results in higher torque ripple.

To evaluate the dynamic performance over the entire speed range, the final comparative experiment demonstrates a full speed reverse test. Fig. 12 shows the results of rotating speed, electromagnetic torque, and stator current of all methods, respectively. As can be seen from the figure, all methods have achieved very similar results. While, FOC shows better current performance, which is the benefit of using the independent inner current PI controller. In the MPTC algorithm, the cost function considers the prediction errors of torque and flux. Therefore, the weighting factor determines the electromagnetic torque performance and the quality of magnetic flux. In summary, all methods in the comparison result can achieve acceptable control performance throughout the entire speed range.

TABLE III
COMPARATIVE ANALYSIS OF EXPERIMENTS

	FOC	DTC	MPTC
Switching Freq.	4 kHz	4 kHz	3.92 kHz
Current THD	3.2%	4.0%	3.6%
Torque SD	0.1473	0.2227	0.1852
Dynamics	2 ms	0.5 ms	0.5 ms

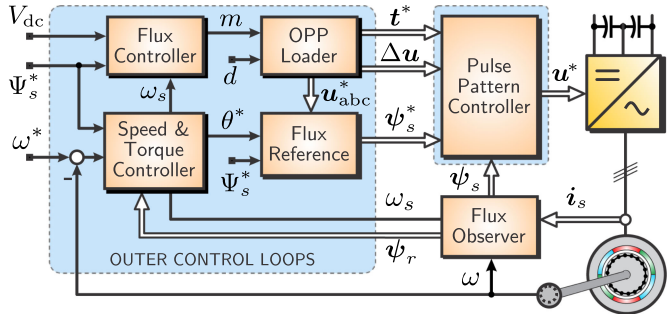

Fig. 13. MP^{3}C scheme based on optimized pulse patterns.

Finally, the performance comparison of the tested control strategies in terms of switching frequency, current THD, torque SD, among other indexes, is summarized in Table III. As shown, the FOC algorithm's steady-state performance is better since, for similar switching frequencies, the current THD and torque ripple are slightly lower. However, in terms of the dynamic performance, the FOC algorithm takes a longer settling time for torque transients when compared with MPTC and DTC strategies. Besides, MPTC can achieve dynamic responses like the DTC while keeping better steady-state performance.

VII. ASSESSMENT OF MPC IN A HIGH POWER DRIVE

A. MP^{3}C Control Strategy

The block diagram of the MP^{3}C strategy is depicted in Fig. 13. This controller combines the modulator and inner control loop in one computational stage using the receding horizon control policy [28]–[34]. From this perspective, for a given input trajectory, an internal model of the drive system allows predicting the system's output trajectory over a prediction horizon. An optimization stage minimizes the stator flux error by manipulating the time-instant of the optimal switching transitions derived from optimum pulse patterns (OPP) [121].

B. Experimental Results

Experimental results for a medium-voltage NPC inverter (dc-link voltage is set to $V_{\rm dc} = 4.84$ kV) driving a 3.3-kV IM rated at 1140 kVA are summarized in this review article (further details can be found in [33]).

Torque steps from 85% to 35% rated torque are shown in Fig. 14. MP^{3}C achieves the same torque settling time as DTC [122], [123], which is below 1 ms. This feature is due to the

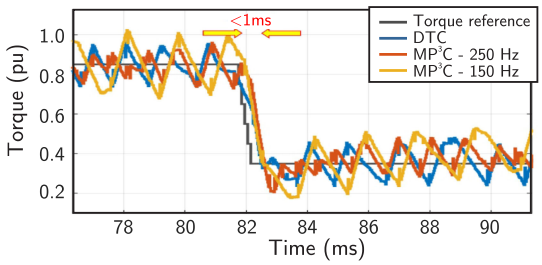

Fig. 14. Medium-voltage experimental results: MP^{3}C and DTC during a torque reference step from 85% to 35% rated torque [33].

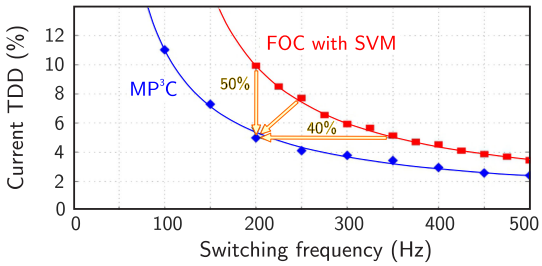

Fig. 15. Simulation results: Current TDD versus switching frequency when comparing FOC-SVM and MP^{3}C (operating at full load), [33].

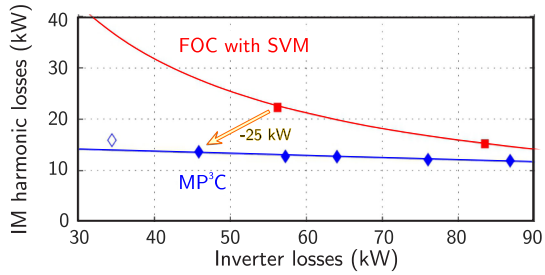

Fig. 16. Simulation results: Tradeoff between the harmonic losses of the IM and the inverter losses, [33].

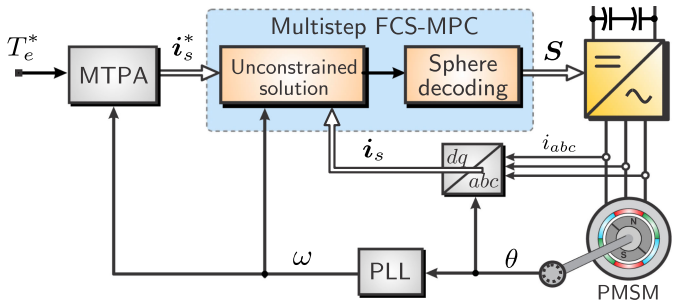

Fig. 17. Multistep model predictive current control for electrical car applications, [35].

insertion of additional switching transitions into the switching pattern in case of large stator flux errors [30].

C. Assessment and Comparison With FOC-SVM

To quantify the user benefits of the MP^{3}C strategy in relation to the standard FOC with SVM, a comprehensive simulation work of an idealized variable speed drive system was done in [33]. The harmonic performance of MP^{3}C with that of FOC-SVM is compared in Fig. 15. As shown, up to 50% lower current distortions or up to 40% lower switching frequency can be obtained by using MP^{3}C. A third alternative is to reduce both the switching frequency and the current distortions. An example of this approach is addressed by the diagonal arrow in Fig. 15. Here, MP^{3}C reduces the switching frequency by 20% and the current TDD by 35%.

As can be concluded from the above analysis, the performance of the drive system can be optimized by adequately reducing the iron and copper losses in the IM and the switching losses in the power converter. Also, low current distortions imply low ripple of the electromagnetic torque, which leads to lower mechanical stress. This feature allows improving the reliability and also enables increasing the maintenance intervals to reduce the operational costs of the drive system.

In an effort to quantify these benefits, detailed simulations of a 3.3-kV drive system with a 10.3-MW IM were carried out (further details in [33]). The tradeoff between the inverter losses and the harmonic losses of the machine is shown in Fig. 16 when varying the switching frequency at nominal speed and load. It is clear from the results that MP^{3}C achieves a superior performance in terms of losses. As indicated by the arrow in Fig. 16, MP^{3}C at $f_{\rm sw}$=150 Hz achieves a total loss reduction of 25 kW with respect to SVM at $f_{\rm sw}$=250 Hz. This loss reduction can have a significant impact on both the capital expenditure as well as the operating costs of the system. For instance, by considering an electricity price of 80€ per MWh, the operational cost of the whole drive system can be reduced by 21k € per year, [33].

VIII. Assessment of MPC for Electric Vehicles Application

The implementation of predictive control for a multistep prediction, or also known as long-horizon prediction, has been proposed as a control strategy in power electronics, [124]. The main characteristics of this method is its ability to work with lower switching frequency, reducing the losses of the inverter in comparison with PWM [125]–[127]. This last characteristic has allowed it to position itself as an attractive strategy for electromobility applications, where energy efficiency is essential, [35]. Sphere decoding allows one to solve the underlying integer optimization problem in a computationally efficient way [128], [129].

The proposed multistep strategy with sphere decoding in [35] is shown in Fig. 17. The proposed method was implemented in a two-level VSI feeding a interior-PMSM which is a typical electrical drive system for electrical car. In this article, the cost function used is

$$g = \sum_{k=t}^{t+N} (1-\lambda_u)\left\|\Delta \boldsymbol{i}_{dq}^{k+1}\right\|_2^2 + \lambda_u \left\|\Delta \boldsymbol{u}^k\right\|_2^2 \qquad (18)$$

where the control objectives are the direct and quadrature machine currents along with the change in the three-phase switching positions to minimize the commutations.

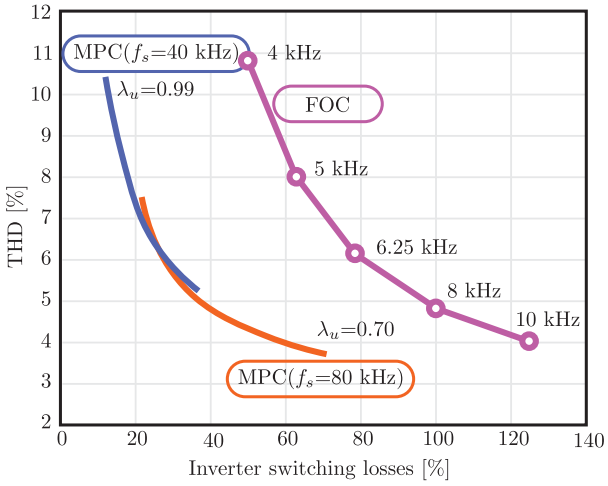

Fig. 18. Inverter switching losses versus THD, reproduced from [35]. Here, f_s refers to the sampling frequency.

TABLE IV
MEASUREMENTS SHOWING THE TOTAL INVERTER LOSSES DIFFERENCE
$\Delta P = 100 \times (P_{\mathrm{MPC}} - P_{\mathrm{FOC}})/P_{\mathrm{FOC}}$

Load Torque (N.m)	Speed (r/min) 1000	2000	3000	4000
10	-26%	-14%	-13%	-14%
20	-20%	-9%	-9%	-13%
30	-16%	-6%	-7%	-12%
40	-10%	-5%	-6%	-11%
50	-7%	-4%	-6%	-10%

The efficiency in the use of energy is crucial today. This becomes even more important in electromobility applications, where the available energy is limited, as is the case with an electric car. Fig. 18 shows the performance of multistep strategy, where it can be seen that it is possible to reduce the losses in the converter for the same harmonic distortion.

Table IV presents a comparison between the inverter losses generated by MPC and FOC in a wide operating range, that it is a summary of the Fig. 8 of [35]. FOC method always generates greater losses in the inverter. Around nominal speed and nominal torque this difference is smaller, however, in other operating points this difference is very significant.

Another important requirement for a control scheme in an electromobility application is to reduce the vibrations it generates. In [35], it is shown that the acoustic noise generated by MPC is comparable to linear controller with PWM.

IX. CHALLENGES AND FUTURE WORK

Until now, MPC has shown that it can be applied in a variety of electrical machines using commercially available microprocessors. And that it works well. The main challenge for MPC is to be adopted by the industry and to achieve this goal it must demonstrate that it offers some advantages in relation to linear control with PWM, which is the standard solution. What the industry demands from the control strategy is as follows.

1) Ease of application.
2) An increase in inverter efficiency.
3) Reduction in the distortion of the current supplied to the motor.
4) Control of acoustic noise, very important in electric cars.
5) Robust behavior against parameter mismatch.
6) Be implemented with standard microprocessors.
7) Applicability to a wide range of converter systems, including grid-connected converters, as well as inverter drive systems.

All these aspects must be addressed in future research. In addition, future work should make a very careful comparison with FOC, using linear controllers and PWM and where possible, to demonstrate that it can achieve better results. The comparison must be made independently for each application, converter, and motor type. A good result on a drive with a 10-kW induction machine will not necessarily be the best on a 10-MW synchronous machine.

X. CONCLUSION

The results presented in this article show that MPC can be adapted to control a wide variety of electrical machines, maintaining the simplicity of the basic control strategy. Particular restrictions and conditions associated with the different types of machines can be easily included by introducing minor changes in the cost functions. Speed, torque, and flux are well controlled in all applications.

A general assessment of the dynamic behavior of the controlled machine shows that MPC reaches better results than two well-established high-performance strategies, namely, FOC and DTC.

A more specific assessment in a high-power machine driven by a three-level NPC inverter shows that the strategy known as MP^{3}C has superior performance, reducing the inverter losses, and the distortion in the motor current when compared with the classical solutions.

Another specific assessment for electric cars shows that multistep MPCC has an outstanding behavior generating less current distortion in the motor, reducing the inverter losses, with a comparable acoustic noise, compared with classical linear control.

As the main conclusion, it can be affirmed that MPC emerges as a brilliant and competitive alternative to high-performance strategies for the control of electrical machines.

REFERENCES

[1] S. Enyedi, "Electric cars—Challenges and trends," in *Proc. IEEE Int. Conf. Automat., Qual. Testing, Robot.*, 2018, pp. 1–8.
[2] F. Altun, S. A. Tekin, S. Gürel, and M. Cernat, "Design and optimization of electric cars—A review of technological advances," in *Proc. 8th Int. Conf. Renewable Energy Res. Appl.*, 2019, pp. 645–650.
[3] A. Emadi, *Advanced Electric Drive Vehicles*, 1st ed. Boca Raton, FL, USA: CRC Press, Mar. 2014.
[4] S. Rachev, D. Stefanov, L. Dimitrov, and D. Koeva, "Evaluation of electric power losses of an induction motor driving a compact electric vehicle at change of parameters and loads," in *Proc. Electr. Veh. Int. Conf.*, 2019, pp. 1–5.

[5] C. Jiang, M. Qiao, P. Zhu, and Q. Zheng, "Design and verification of high speed permanent magnet synchronous motor for electric car," in *Proc. 2nd IEEE Adv. Inf. Manage., Communicates, Electron. Automat. Control Conf.*, 2018, pp. 2371–2375.

[6] F. Zuo, X. Zhang, Y. Zhu, Y. Xu, X. Lv, and C. Qian, "The simulation analysis of control system of pure electric pick-up truck motor," in *Proc. IEEE 3rd Adv. Inf. Technol., Electron. Automat. Control Conf.*, 2018, pp. 1704–1711.

[7] M. Islameka, I. N. Haq, E. Leksono, and B. Yuliarto, "Energy consumption simulation and analysis of rear-driven electric bus with regenerative braking," in *Proc. 6th Int. Conf. Electr. Veh. Technol.*, 2019, pp. 105–110.

[8] Z. Ke, J. Zhang, and M. W. Degner, "DC bus capacitor discharge of permanent-magnet synchronous machine drive systems for hybrid electric vehicles," *IEEE Trans. Ind. Appl.*, vol. 53, no. 2, pp. 1399–1405, Mar./Apr. 2017.

[9] P. Suwanapingkarl, A. Loongthaisong, N. Ritsuk, S. Buasai, C. Paorung, and K. Srivallop, "Motor design for 'ePVScooter' an electric scooter integrated with portable photovoltaic charger system," in *Proc. Int. Conf. Power, Energy Innov.*, 2019, pp. 1–3.

[10] Y. U. Nugraha, M. N. Yuniarto, H. Herizal, D. A. Asfani, D. C. Riawan, and M. Wahyudi, "Design analysis of axial flux permanent magnet BLDC motor 5 kW for electric scooter application," in *Proc. Int. Seminar Intell. Technol. Appl.*, 2018, pp. 163–168.

[11] L. Wu, W. Ding, and Y. Hu, "Design and analysis of an external-rotor switched reluctance machine for electric bicycle," in *Proc. 11th Int. Conf. Ecol. Veh. Renewable Energies*, 2016, pp. 1–6.

[12] G. Sieklucki, "An investigation into the induction motor of Tesla model S vehicle," in *Proc. Int. Symp. Elect. Mach.*, 2018, pp. 1–6.

[13] E. Sokolov, "Comparative study of electric car traction motors," in *Proc. 15th Int. Conf. Elect. Mach., Drives Power Syst.*, 2017, pp. 348–353.

[14] P. Rafajdus, A. Peniak, M. Diko, J. Makarovic, P. Dubravka, and V. Hrabovcova, "Using of suitable reluctance motors for electric vehicles and comparison of their performances," in *Proc. IEEE 15th Int. Conf. Environ. Elect. Eng.*, 2015, pp. 2056–2060.

[15] F. Blaschke, "Apparatus for field-oriented control of asynchronous machines," U.S. Patent US00283404A, Apr. 1971. [Online]. Available: https://patents.google.com/patent/US3805135A/en

[16] F. Blaschke, "The principle of field orientation as applied to the new transvector closed-loop system for rotating-field machines," *Siemens Rev.*, vol. 34, no. 3, pp. 217–220, 1972.

[17] F. Wang, Z. Zhang, X. Mei, J. Rodríguez, and R. Kennel, "Advanced control strategies of induction machine: Field oriented control, direct torque control and model predictive control," *Energies*, vol. 11, no. 1, Jan. 2018, Art. no. 120.

[18] F. Wang, X. Mei, J. Rodriguez, and R. Kennel, "Model predictive control for electrical drive systems—An overview," *CES Trans. Elect. Mach. Syst.*, vol. 1, no. 3, pp. 219–230, 2017.

[19] S. Kouro, M. A. Perez, J. Rodriguez, A. M. Llor, and H. A. Young, "Model predictive control: MPC's role in the evolution of power electronics," *IEEE Ind. Electron. Mag.*, vol. 9, no. 4, pp. 8–21, Dec. 2015.

[20] T. Geyer, *Model Predictive Control of High Power Converters and Industrial Drives*, 1st ed. Hoboken, NJ, USA: Wiley, 2016.

[21] P. Karamanakos, E. Liegmann, T. Geyer, and R. Kennel, "Model predictive control of power electronic systems: Methods, results, and challenges," *IEEE Open J. Ind. Appl.*, vol. 1, pp. 95–114, 2020.

[22] M. Norambuena, J. Rodriguez, Z. Zhang, F. Wang, C. Garcia, and R. Kennel, "A very simple strategy for high-quality performance of AC machines using model predictive control," *IEEE Trans. Power Electron.*, vol. 34, no. 1, pp. 794–800, Jan. 2019.

[23] L. Chen, S. Huang, J. Guo, Z. Hu, X. Fu, and G. Cao, "Model predictive position control for a planar switched reluctance motor using parametric regression model," in *Proc. IEEE Int. Symp. Predictive Control Elect. Drives Power Electron.*, 2019, pp. 1–4.

[24] X. Wang, F. Niu, X. Huang, L. Wu, K. Li, and Y. Fang, "Model parameter online correction method of predictive current control for permanent magnet synchronous motor," in *Proc. 22nd Int. Conf. Elect. Mach. Syst.*, 2019, pp. 1–4.

[25] Y. Zhang, Z. Yin, W. Li, X. Tong, and Y. Zhong, "Speed sensorless model predictive control based on disturbance observer for induction motor drives," in *Proc. IEEE Int. Symp. Predictive Control Elect. Drives Power Electron.*, 2019, pp. 1–4.

[26] R. Xue, D. Xu, J. Ji, and T. Tao, "Robustness improvement of two-vector-based model predictive current control for permanent magnet synchronous motor," in *Proc. 22nd Int. Conf. Elect. Mach. Syst.*, 2019, pp. 1–5.

[27] P. G. Carlet, F. Toso, A. Favato, and S. Bolognani, "A speed and current cascade continuous control set model predictive control architecture for synchronous motor drives," in *Proc. IEEE Energy Convers. Congr. Expo.*, 2019, pp. 5682–5688.

[28] T. Geyer, N. Oikonomou, G. Papafotiou, and F. Kieferndorf, "Model predictive pulse pattern control," in *Proc. IEEE Energy Convers. Congr. Expo.*, 2011, pp. 3306–3313.

[29] T. Geyer, N. Oikonomou, G. Papafotiou, and F. D. Kieferndorf, "Model predictive pulse pattern control," *IEEE Trans. Ind. Appl.*, vol. 48, no. 2, pp. 663–676, Mar./Apr. 2012.

[30] T. Geyer and N. Oikonomou, "Model predictive pulse pattern control with very fast transient responses," in *Proc. IEEE Energy Convers. Congr. Expo.*, 2014, pp. 5518–5524.

[31] N. Oikonomou, C. Gutscher, P. Karamanakos, F. D. Kieferndorf, and T. Geyer, "Model predictive pulse pattern control for the five-level active neutral-point-clamped inverter," *IEEE Trans. Ind. Appl.*, vol. 49, no. 6, pp. 2583–2592, Nov./Dec. 2013.

[32] S. Richter, T. Geyer, and M. Morari, "Resource-efficient gradient methods for model predictive pulse pattern control on an FPGA," *IEEE Trans. Control Syst. Technol.*, vol. 25, no. 3, pp. 828–841, May 2017.

[33] T. Geyer, V. Spudic, W. van der Merwe, and E. Guidi, "Model predictive pulse pattern control of medium-voltage neutral-point-clamped inverter drives," in *Proc. IEEE Energy Convers. Congr. Expo.*, 2018, pp. 5047–5054.

[34] M. Vasiladiotis, A. Christe, and T. Geyer, "Model predictive pulse pattern control for modular multilevel converters," *IEEE Trans. Ind. Electron.*, vol. 66, no. 3, pp. 2423–2431, Mar. 2019.

[35] A. Andersson and T. Thiringer, "Assessment of an improved finite control set model predictive current controller for automotive propulsion applications," *IEEE Trans. Ind. Electron.*, vol. 67, no. 1, pp. 91–100, Jan. 2020.

[36] M. Rivera, J. Rodriguez, and S. Vazquez, "Predictive control in power converters and electrical drives—Part I," *IEEE Trans. Ind. Electron.*, vol. 63, no. 6, pp. 3834–3836, Jun. 2016.

[37] J. Holtz, "A predictive controller for the stator current vector of AC machines fed from a switched voltage source," in *Proc. IEE Jpn. Int. Power Electron. Conf.-Tokyo*, 1983, pp. 1665–1675.

[38] M. Depenbrock, "Direct self-control (DSC) of inverter-fed induction machine," *IEEE Trans. Power Electron.*, vol. 3, no. 4, pp. 420–429, Oct. 1988.

[39] E. Flach, R. Hoffmann, and P. Mutschler, "Direct mean torque control of an induction motor," in *Proc. Eur. Conf. Power Electron. Appl.*, vol. 3, 1997, pp. 672–677.

[40] P. Cortes, M. P. Kazmierkowski, R. M. Kennel, D. E. Quevedo, and J. Rodriguez, "Predictive control in power electronics and drives," *IEEE Trans. Ind. Electron.*, vol. 55, no. 12, pp. 4312–4324, Dec. 2008.

[41] I. Takahashi and T. Noguchi, "A new quick-response and high-efficiency control strategy of an induction motor," *IEEE Trans. Ind. Appl.*, vol. IA- 22, no. 5, pp. 820–827, Sep. 1986.

[42] S. A. Davari, F. Wang, and R. M. Kennel, "Robust deadbeat control of an induction motor by stable MRAS speed and stator estimation," *IEEE Trans. Ind. Informat.*, vol. 14, no. 1, pp. 200–209, Jan. 2018.

[43] J. Stumper, V. Hagenmeyer, S. Kuehl, and R. Kennel, "Deadbeat control for electrical drives: A robust and performant design based on differential flatness," *IEEE Trans. Power Electron.*, vol. 30, no. 8, pp. 4585–4596, Aug. 2015.

[44] L. Yan, M. Dou, Z. Hua, H. Zhang, and J. Yang, "Optimal duty cycle model predictive current control of high-altitude ventilator induction motor with extended minimum stator current operation," *IEEE Trans. Power Electron.*, vol. 33, no. 8, pp. 7240–7251, Aug. 2018.

[45] C. Xu, Z. Han, and S. Lu, "Deadbeat predictive current control for permanent magnet synchronous machines with closed-form error compensation," *IEEE Trans. Power Electron.*, vol. 35, no. 5, pp. 5018–5030, May 2020.

[46] Y. Zhang, J. Jin, and L. Huang, "Model-free predictive current control of PMSM drives based on extended state observer using ultra-local model," *IEEE Trans. Ind. Electron.*, vol. 68, no. 2, pp. 993–1003, Feb. 2021.

[47] Z. Song, F. Zhou, and Z. Zhang, "Parallel-observer-based predictive current control of permanent magnet synchronous machines with reduced switching frequency," *IEEE Trans. Ind. Informat.*, vol. 15, no. 12, pp. 6457–6467, Dec. 2019.

[48] K. Lee and F. Blaabjerg, "Sensorless DTC-SVM for induction motor driven by a matrix converter using a parameter estimation strategy," *IEEE Trans. Ind. Electron.*, vol. 55, no. 2, pp. 512–521, Feb. 2008.

[49] S. A. Davari, D. A. Khaburi, F. Wang, and R. M. Kennel, "Using full order and reduced order observers for robust sensorless predictive torque control of induction motors," *IEEE Trans. Power Electron.*, vol. 27, no. 7, pp. 3424–3433, Jul. 2012.

[50] R. Errouissi, M. Ouhrouche, W.-H. Chen, and A. M. Trzynadlowski, "Robust nonlinear predictive controller for permanent-magnet synchronous motors with an optimized cost function," *IEEE Trans. Ind. Electron.*, vol. 59, no. 7, pp. 2849–2858, Jul. 2012.

[51] T. Türker, U. Buyukkeles, and A. F. Bakan, "A robust predictive current controller for PMSM drives," *IEEE Trans. Ind. Electron.*, vol. 63, no. 6, pp. 3906–3914, Jun. 2016.

[52] R. Kennel, A. Linder, and M. Linke, "Generalized predictive control (GPC)-ready for use in drive applications?," in *Proc. IEEE 32nd Annu. Power Electron. Specialists Conf.*, 2001, vol. 4, pp. 1839–1844.

[53] F. Wang, L. He, and J. Rodriguez, "FPGA-based continuous control set model predictive current control for PMSM system using multistep error tracking technique," *IEEE Trans. Power Electron.*, vol. 35, no. 12, pp. 13455–13464, Dec. 2020.

[54] A. A. Ahmed, B. K. Koh, and Y. I. Lee, "A comparison of finite control set and continuous control set model predictive control schemes for speed control of induction motors," *IEEE Trans. Ind. Informat.*, vol. 14, no. 4, pp. 1334–1346, Apr. 2018.

[55] X. Luo, A. Shen, Q. Tang, J. Liu, and J. Xu, "Two-step continuous-control set model predictive current control strategy for SPMSM sensorless drives," *IEEE Trans. Energy Convers.*, vol. 36, no. 2, pp. 1110–1120, Jun. 2021.

[56] D. Kouzoupis, A. Zanelli, H. Peyrl, and H. J. Ferreau, "Towards proper assessment of QP algorithms for embedded model predictive control," in *Proc. Eur. Control Conf.*, 2015, pp. 2609–2616.

[57] G. Cimini, D. Bernardini, S. Levijoki, and A. Bemporad, "Embedded model predictive control with certified real-time optimization for synchronous motors," *IEEE Trans. Control Syst. Technol.*, vol. 29, no. 2, pp. 893–900, Mar. 2021.

[58] J. Rodriguez *et al.*, "Predictive current control of a voltage source inverter," *IEEE Trans. Ind. Electron.*, vol. 54, no. 1, pp. 495–503, Feb. 2007.

[59] S. Kouro, P. Cortes, R. Vargas, U. Ammann, and J. Rodriguez, "Model predictive control—A simple and powerful method to control power converters," *IEEE Trans. Ind. Electron.*, vol. 56, no. 6, pp. 1826–1838, Jun. 2009.

[60] A. Mora, Orellana, J. Juliet, and R. Cárdenas, "Model predictive torque control for torque ripple compensation in variable-speed PMSMs," *IEEE Trans. Ind. Electron.*, vol. 63, no. 7, pp. 4584–4592, Jul. 2016.

[61] H. Miranda, P. Cortes, J. I. Yuz, and J. Rodriguez, "Predictive torque control of induction machines based on state-space models," *IEEE Trans. Ind. Electron.*, vol. 56, no. 6, pp. 1916–1924, Jun. 2009.

[62] A. A. Ahmed, "Fast-speed drives for permanent magnet synchronous motor based on model predictive control," in *Proc. IEEE Veh. Power Propul. Conf.*, 2015, pp. 1–6.

[63] P. Karamanakos, P. Stolze, R. M. Kennel, S. Manias, and H. du T. Mouton, "Variable switching point predictive torque control of induction machines," *IEEE Trans. Emerg. Sel. Topics Power Electron.*, vol. 2, no. 2, pp. 285–295, Jun. 2014.

[64] A. A. Ahmed, B. K. Koh, H. S. Park, K. Lee, and Y. I. Lee, "Finite-control set model predictive control method for torque control of induction motors using a state tracking cost index," *IEEE Trans. Ind. Electron.*, vol. 64, no. 3, pp. 1916–1928, Mar. 2017.

[65] S. A. Davari, M. Norambuena, V. Nekoukar, C. Garcia, and J. Rodriguez, "Even-handed sequential predictive torque and flux control," *IEEE Trans. Ind. Electron.*, vol. 67, no. 9, pp. 7334–7342, Sep. 2020.

[66] Y. Zhang and H. Yang, "Model-predictive flux control of induction motor drives with switching instant optimization," *IEEE Trans. Energy Convers.*, vol. 30, no. 3, pp. 1113–1122, Sep. 2015.

[67] M. Siami, D. Arab Khaburi, and J. Rodriguez, "Simplified finite control set-model predictive control for matrix converter-fed PMSM drives," *IEEE Trans. Power Electron.*, vol. 33, no. 3, pp. 2438–2446, Mar. 2018.

[68] V. P. Muddineni, S. R. Sandepudi, and A. K. Bonala, "Finite control set predictive torque control for induction motor drive with simplified weighting factor selection using TOPSIS method," *IET Electr. Power Appl.*, vol. 11, no. 5, pp. 749–760, 2017.

[69] E. Fuentes, C. A. Silva, and R. M. Kennel, "MPC implementation of a quasi-time-optimal speed control for a PMSM drive, with inner modulated-FS-MPC torque control," *IEEE Trans. Ind. Electron.*, vol. 63, no. 6, pp. 3897–3905, Jun. 2016.

[70] C. F. Garcia, C. A. Silva, J. R. Rodriguez, P. Zanchetta, and S. A. Odhano, "Modulated model-predictive control with optimized overmodulation," *IEEE Trans. Emerg. Sel. Topics Power Electron.*, vol. 7, no. 1, pp. 404–413, Mar. 2019.

[71] A. Mora, F. Donoso, M. Urrutia, A. Angulo, and R. Cárdenas, "Predictive control strategy for an induction machine fed by a 3L-NPC converter with fixed switching frequency and improved tracking error," in *Proc. IEEE 27th Int. Symp. Ind. Electron.*, 2018, pp. 155–160.

[72] I. Kim, R. Chan, and S. Kwak, "Model predictive control method for CHB multi-level inverter with reduced calculation complexity and fast dynamics," *IET Electr. Power Appl.*, vol. 11, no. 5, pp. 784–792, 2017.

[73] B. Bilgin and A. Emadi, "Electric motor industry and switched reluctance machines," in *Switched Reluctance Motor Drives: Fundamentals to Applications*. Boca Raton, FL, USA: CRC Press, 2018, ch. 1, pp. 1–34.

[74] H. Chen, S. Xu, and S. Cui, "Reliability evaluation for power converter of SRM on fault-tolerate capability and thermal stress," *IEEE Trans. Ind. Electron.*, vol. 68, no. 2, pp. 1749–1758, Feb. 2021.

[75] J.-W. Ahn and G. F. Lukman, "Switched reluctance motor: Research trends and overview," *CES Trans. Elect. Mach. Syst.*, vol. 2, no. 4, pp. 339–347, Dec. 2018.

[76] B. Burkhart, A. Klein-Hessling, I. Ralev, C. P. Weiss, and R. W. D. Doncker, "Technology, research and applications of switched reluctance drives," *CPSS Trans. Power Electron. Appl.*, vol. 2, no. 1, pp. 12–27, 2017.

[77] B. Bilgin *et al.*, "Making the case for switched reluctance motors for propulsion applications," *IEEE Trans. Veh. Technol.*, vol. 69, no. 7, pp. 7172–7186, Jul. 2020.

[78] S. Ullah, S. P. McDonald, R. Martin, M. Benarous, and G. J. Atkinson, "A permanent magnet assist, segmented rotor, switched reluctance drive for fault tolerant aerospace applications," *IEEE Trans. Ind. Appl.*, vol. 55, no. 1, pp. 298–305, Jan./Feb. 2019.

[79] B. Bilgin and A. Emadi, "Electric motors in electrified transportation: A step toward achieving a sustainable and highly efficient transportation system," *IEEE Power Electron. Mag.*, vol. 1, no. 2, pp. 10–17, Jun. 2014.

[80] J. W. Jiang, "Design considerations for switched reluctance machines," in *Switched Reluctance Motor Drives: Fundamentals to Applications*. Boca Raton, FL, USA: CRC Press, 2018, ch. 7, pp. 253–315.

[81] E. Bostanci, M. Moallem, A. Parsapour, and B. Fahimi, "Opportunities and challenges of switched reluctance motor drives for electric propulsion: A comparative study," *IEEE Trans. Transport. Electrific.*, vol. 3, no. 1, pp. 58–75, Mar. 2017.

[82] S. Li, S. Zhang, T. G. Habetler, and R. G. Harley, "Modeling, design optimization, and applications of switched reluctance machines," *IEEE Trans. Ind. Appl.*, vol. 55, no. 3, pp. 2660–2681, May/Jun. 2019.

[83] J. Ye, B. Bilgin, and A. Emadi, "An offline torque sharing function for torque ripple reduction in switched reluctance motor drives," *IEEE Trans. Energy Convers.*, vol. 30, no. 2, pp. 726–735, Jun. 2015.

[84] H. Li, B. Bilgin, and A. Emadi, "An improved torque sharing function for torque ripple reduction in switched reluctance machines," *IEEE Trans. Power Electron.*, vol. 34, no. 2, pp. 1635–1644, Feb. 2019.

[85] A. D. Callegaro, B. Bilgin, and A. Emadi, "Radial force shaping for acoustic noise reduction in switched reluctance machines," *IEEE Trans. Power Electron.*, vol. 34, no. 10, pp. 9866–9878, Oct. 2019.

[86] D. F. Valencia, S. R. Filho, A. D. Callegaro, M. Preindl, and A. Emadi, "Virtual-flux finite control set model predictive control of switched reluctance motor drives," in *Proc. 45th Annu. Conf. IEEE Ind. Electron. Soc.*, Oct. 2019, vol. 1, pp. 1465–1470.

[87] X. Li and P. Shamsi, "Model predictive current control of switched reluctance motors with inductance auto-calibration," *IEEE Trans. Ind. Electron.*, vol. 63, no. 6, pp. 3934–3941, Jun. 2016.

[88] C. Li, G. Wang, Y. Li, and A. Xu, "An improved finite-state predictive torque control for switched reluctance motor drive," *IET Electr. Power Appl.*, vol. 12, no. 1, pp. 144–151, 2018.

[89] R. Abdel-Fadil and L. Számel, "Enhancement of the switched reluctance motor performance for electric vehicles applications using predictive current control," in *Proc. Int. IEEE Conf. Workshop Óbuda Elect. Power Eng.*, Nov. 2018, pp. 195–200.

[90] S. Song, R. Hei, R. Ma, and W. Liu, "Model predictive control of switched reluctance starter/generator with torque sharing and compensation," *IEEE Trans. Transport. Electrific.*, vol. 6, no. 4, pp. 1519–1527, Dec. 2020.

[91] R. Tarvirdilu-Asl, S. Nalakath, B. Bilgin, and A. Emadi, "A finite control set model predictive torque control for switched reluctance motor drives with adaptive turn-off angle," in *Proc. 45th Annu. Conf. IEEE Ind. Electron. Soc.*, Oct. 2019, vol. 1, pp. 840–845.

[92] X. Li and P. Shamsi, "Inductance surface learning for model predictive current control of switched reluctance motors," *IEEE Trans. Transport. Electrific.*, vol. 1, no. 3, pp. 287–297, Oct. 2015.
[93] M. G. Bijan, M. Al-Badri, P. Pillay, and P. Angers, "Induction machine parameter range constraints in genetic algorithm based efficiency estimation techniques," *IEEE Trans. Ind. Appl.*, vol. 54, no. 5, pp. 4186–4197, Sep./Oct. 2018.
[94] K. Wang, Y. Li, Q. Ge, and L. Shi, "An improved indirect field-oriented control scheme for linear induction motor traction drives," *IEEE Trans. Ind. Electron.*, vol. 65, no. 12, pp. 9928–9937, Dec. 2018.
[95] W. Xu, R. Islam, and M. Pucci, *Advanced Linear Machines and Drive Systems*, 1st ed. Berlin, Germany: Springer, Aug. 2019.
[96] W. Xu, J. Zou, Y. Liu, and J. Zhu, "Weighting factorless model predictive thrust control for linear induction machine," *IEEE Trans. Power Electron.*, vol. 34, no. 10, pp. 9916–9928, Oct. 2019.
[97] J. Zou, W. Xu, X. Yu, Y. Liu, and C. Ye, "Multistep model predictive control with current and voltage constraints for linear induction machine based urban transportation," *IEEE Trans. Veh. Technol.*, vol. 66, no. 12, pp. 10817–10829, Dec. 2017.
[98] J. Zou, W. Xu, J. Zhu, and Y. Liu, "Low-complexity finite control set model predictive control with current limit for linear induction machines," *IEEE Trans. Ind. Electron.*, vol. 65, no. 12, pp. 9243–9254, Dec. 2018.
[99] J. Zou, W. Xu, J. Zhu, and Y. Liu, "Simplified model predictive thrust control based arbitrary two voltage vectors for linear induction machines in metro transportation," *IEEE Trans. Veh. Technol.*, vol. 69, no. 7, pp. 7092–7103, Jul. 2020.
[100] J. Zou, W. Xu, and C. Ye, "Improved deadbeat control strategy for linear induction machine," *IEEE Trans. Magn.*, vol. 53, no. 6, Jun. 2017, Art. no. 8106804.
[101] J. Zou and W. Xu, "Optimal current reference with maximum thrust criterion for linear induction machine based deadbeat control," in *Proc. 43rd Annu. Conf. IEEE Ind. Electron. Soc.*, 2017, pp. 3682–3687.
[102] W. Xu, M. F. Elmorshedy, Y. Liu, M. R. Islam, and S. M. Allam, "Finite-set model predictive control based thrust maximization of linear induction motors used in linear metros," *IEEE Trans. Veh. Technol.*, vol. 68, no. 6, pp. 5443–5458, Jun. 2019.
[103] W. Xu, M. F. Elmorshedy, Y. Liu, J. Rodriguez, and C. Garcia, "Maximum thrust per ampere of linear induction machine based on finite-set model predictive direct thrust control," *IEEE Trans. Power Electron.*, vol. 35, no. 7, pp. 7366–7378, Jul. 2020.
[104] M. Elmorshedy, W. Xu, S. M. Allam, J. Rodriguez, and C. Garcia, "MTPA-based finite-set model predictive control without weighting factors for linear induction machine," *IEEE Trans. Ind. Electron.*, vol. 68, no. 3, pp. 2034–2047, Mar. 2021.
[105] F. Barrero and M. J. Duran, "Recent advances in the design, modeling, and control of multiphase machines—Part I," *IEEE Trans. Ind. Electron.*, vol. 63, no. 1, pp. 449–458, Jan. 2016.
[106] M. J. Duran and F. Barrero, "Recent advances in the design, modeling, and control of multiphase machines—Part II," *IEEE Trans. Ind. Electron.*, vol. 63, no. 1, pp. 459–468, Jan. 2016.
[107] E. Levi, "Advances in converter control and innovative exploitation of additional degrees of freedom for multiphase machines," *IEEE Trans. Ind. Electron.*, vol. 63, no. 1, pp. 433–448, Jan. 2016.
[108] J. Rodas, F. Barrero, M. R. Arahal, C. Martín, and R. Gregor, "Online estimation of rotor variables in predictive current controllers: A case study using five-phase induction machines," *IEEE Trans. Ind. Electron.*, vol. 63, no. 9, pp. 5348–5356, Sep. 2016.
[109] J. Rodas, C. Martín, M. R. Arahal, F. Barrero, and R. Gregor, "Influence of covariance-based ALS methods in the performance of predictive controllers with rotor current estimation," *IEEE Trans. Ind. Electron.*, vol. 64, no. 4, pp. 2602–2607, Apr. 2017.
[110] M. Ayala, J. Doval-Gandoy, J. Rodas, O. Gonzalez, R. Gregor, and M. Rivera, "A novel modulated model predictive control applied to six-phase induction motor drives," *IEEE Trans. Ind. Electron.*, vol. 68, no. 5, pp. 3672–3682, May 2021.
[111] M. R. Arahal, F. Barrero, M. J. Duran, M. G. Ortega, and C. Martín, "Trade-offs analysis in predictive current control of multi-phase induction machines," *Control Eng. Pract.*, vol. 81, pp. 105–113, 2018.
[112] M. J. Duran, J. A. Riveros, F. Barrero, H. Guzman, and J. Prieto, "Reduction of common-mode voltage in five-phase induction motor drives using predictive control techniques," *IEEE Trans. Ind. Appl.*, vol. 48, no. 6, pp. 2059–2067, Nov./Dec. 2012.
[113] J. A. Riveros, F. Barrero, E. Levi, M. J. Durán, S. Toral, and M. Jones, "Variable-speed five-phase induction motor drive based on predictive torque control," *IEEE Trans. Ind. Electron.*, vol. 60, no. 8, pp. 2957–2968, Aug. 2013.
[114] J. J. Aciego, I. González Prieto, and M. J. Duran, "Model predictive control of six-phase induction motor drives using two virtual voltage vectors," *IEEE Trans. Emerg. Sel. Topics Power Electron.*, vol. 7, no. 1, pp. 321–330, Mar. 2019.
[115] O. Gonzalez, M. Ayala, J. Doval-Gandoy, J. Rodas, R. Gregor, and M. Rivera, "Predictive-fixed switching current control strategy applied to six-phase induction machine," *Energies*, vol. 12, no. 12, 2019, Art. no. 2294.
[116] P. Gonçalves, S. Cruz, and A. Mendes, "Finite control set model predictive control of six-phase asymmetrical machines—An overview," *Energies*, vol. 12, no. 24, 2019, Art. no. 4693.
[117] M. Bermúdez, C. Martín, I. González-Prieto, M. J. Durán, M. R. Arahal, and F. Barrero, "Predictive current control in electrical drives: An illustrated review with case examples using a five-phase induction motor drive with distributed windings," *IET Electr. Power Appl.*, vol. 14, no. 8, pp. 1291–1310, 2020.
[118] J. Rodriguez, R. M. Kennel, J. R. Espinoza, M. Trincado, C. A. Silva, and C. A. Rojas, "High-performance control strategies for electrical drives: An experimental assessment," *IEEE Trans. Ind. Electron.*, vol. 59, no. 2, pp. 812–820, Feb. 2012.
[119] F. Wang, Z. Chen, P. Stolze, R. Kennel, M. Trincado, and J. Rodriguez, "A comprehensive study of direct torque control (DTC) and predictive torque control (PTC) for high performance electrical drives," *Epe J.*, vol. 25, no. 1, pp. 12–21, 2015.
[120] F. Wang, S. Li, X. Mei, W. Xie, J. Rodríguez, and R. M. Kennel, "Model-based predictive direct control strategies for electrical drives: An experimental evaluation of PTC and PCC methods," *IEEE Trans. Ind. Informat.*, vol. 11, no. 3, pp. 671–681, Jun. 2015.
[121] G. S. Buja, "Optimum output waveforms in PWM inverters," *IEEE Trans. Ind. Appl.*, vol. IA-16, no. 6, pp. 830–836, Nov. 1980.
[122] G. S. Buja and M. P. Kazmierkowski, "Direct torque control of PWM inverter-fed AC motors—A survey," *IEEE Trans. Ind. Electron.*, vol. 51, no. 4, pp. 744–757, Aug. 2004.
[123] T. Geyer, G. Papafotiou, and M. Morari, "Model predictive direct torque control—Part I: Concept, algorithm, and analysis," *IEEE Trans. Ind. Electron.*, vol. 56, no. 6, pp. 1894–1905, Jun. 2009.
[124] T. Geyer and D. E. Quevedo, "Multistep finite control set model predictive control for power electronics," *IEEE Trans. Power Electron.*, vol. 29, no. 12, pp. 6836–6846, Dec. 2014.
[125] A. Ayad, P. Karamanakos, and R. Kennel, "Direct model predictive current control strategy of quasi-Z-source inverters," *IEEE Trans. Power Electron.*, vol. 32, no. 7, pp. 5786–5801, Jul. 2017.
[126] P. Acuna, C. A. Rojas, R. Baidya, R. P. Aguilera, and J. E. Fletcher, "On the impact of transients on multistep model predictive control for medium-voltage drives," *IEEE Trans. Power Electron.*, vol. 34, no. 9, pp. 8342–8355, Sep. 2019.
[127] T. Geyer and D. E. Quevedo, "Performance of multistep finite control set model predictive control for power electronics," *IEEE Trans. Power Electron.*, vol. 30, no. 3, pp. 1633–1644, Mar. 2015.
[128] T. Dorfling, H. du Toit Mouton, T. Geyer, and P. Karamanakos, "Long-horizon finite-control-set model predictive control with nonrecursive sphere decoding on an FGPA," *IEEE Trans. Power Electron.*, vol. 35, no. 7, pp. 7520–7531, Jul. 2020.
[129] P. Karamanakos and T. Geyer, "Guidelines for the design of finite control set model predictive controllers," *IEEE Trans. Power Electron.*, vol. 35, no. 7, pp. 7434–7450, Jul. 2020.

Jose Rodriguez's photograph and biography not available at the time of publication.

Cristian Garcia's photograph and biography not available at the time of publication.

Andres Mora's photograph and biography not available at the time of publication.

S. Alireza Davari's photograph and biography not available at the time of publication.

Jorge Rodas (Senior Member, IEEE) received the M.Sc. degrees from the Universidad de Vigo, Pontevedra, Spain, and the Universidad de Sevilla, Seville, Spain, in 2012 and 2013, respectively, and the joint-university Ph.D. degree from the Universidad Nacional de Asunción, San Lorenzo, Paraguay, and the Universidad de Sevilla, in 2016.

In 2011, he joined the Universidad Nacional de Asuncion, where he is currently a Professor. His research interests include the applications of advanced control to real-world problems. His research interests include applying model-based predictive control and nonlinear control to power electronic converters, renewable energy conversion systems, electric motor drives, and robotic systems (especially drones).

Diego Fernando Valencia (Member, IEEE) received the Ph.D. degree in electrical engineering from McMaster University, Hamilton, ON, Canada, in 2021.

He is currently a Postdoctoral Research Fellow with McMaster Automotive Resource Center (MARC), Hamilton, ON, Canada. His research interests include control of electric motor drives and power electronics for electrified transportation and model predictive control of power converters and drives.

Mahmoud Elmorshedy (Member, IEEE) was born in Gharbeya, Egypt, in 1989. He received the B.Sc. and M.Sc. degrees in electrical engineering from Tanta University, Tanta, Egypt, in 2012 and 2016, and the Ph.D. degree from the Huazhong University of Science and Technology, Wuhan, China, in 2020, respectively.

He started working as a Teaching Assistant with the Department of Electrical Power and Machines Engineering, Tanta University, in 2013. In June 2016, he was promoted to the degree of Assistant Lecturer with the same department. He is currently working as an Assistant Professor with the Department of Electrical Power and Machines Engineering, Faculty of Engineering, Tanta University. His research interests include linear induction motor, predictive control, power electronics, and renewable energy.

Fengxiang Wang's photograph and biography not available at the time of publication.

Kunkun Zuo received the M.S. degree in control engineering from the University of Chinese Academy of Sciences, Beijing, China. He is currently working toward the Ph.D. degree with the Institute of Electrical Drive Systems and Power Electronics, Technical University of Munich, Munich, Germany.

His research interests include model predictive control, disturbance observer, and power optimization control for electrical drive systems.

Luca Tarisciotti's photograph and biography not available at the time of publication.

Freddy Flores-Bahamonde's photograph and biography not available at the time of publication.

Wei Xu (Senior Member, IEEE) received the double B.E. and M.E. degrees from Tianjin University, Tianjin, China, in 2002 and 2005, and the Ph.D. degree from the Institute of Electrical Engineering, Chinese Academy of Sciences, Beijing, China, in 2008, respectively, all in electrical engineering.

His research interests include cover design and control of linear/rotary machines. From 2008 to 2012, he made a Postdoctoral Fellow with the University of Technology Sydney, Ultimo, Austalia, Vice Chancellor Research Fellow with the Royal Melbourne Institute of Technology, Japan Science Promotion Society Invitation Fellow with Meiji University, Tokyo, Japan, respectively. Since 2013, he has been a Full Professor with the State Key Laboratory of Advanced Electromagnetic Engineering, Huazhong University of Science and Technology, Wuhan, China. He has authored more than 110 papers accepted or published in IEEE Journals, two edited books published by Springer Press, one monograph published by China Machine Press, and more than 150 Invention Patents granted or in pending, all in the related fields of electrical machines and drives.

Dr. Xu is the Fellow of the Institute of Engineering and Technology. He is the General Chair for 2021 International Symposium on Linear Drives for Industry Applications (LDIA 2021) and 2023 IEEE International Conference on Predictive Control of Electrical Drives and Power Electronics (PRECEDE 2023) in Wuhan, China, respectively. He has been an Associate Editor for several leading IEEE Transactions Journals, such as IEEE TRANSACTIONS ON INDUSTRIAL ELECTRONICS, IEEE TRANSACTIONS ON VEHICULAR TECHNOLOGY, IEEE TRANSACTIONS ON ENERGY CONVERSION, and so on.

Zhenbin Zhang's photograph and biography not available at the time of publication.

Yongchang Zhang's photograph and biography not available at the time of publication.

Margarita Norambuena's photograph and biography not available at the time of publication.

Ali Emadi (Fellow, IEEE) received the B.S. and M.S. degrees with highest distinction from the Sharif University of Technology, Tehran, Iran, in 1995 and 1997, respectively, and the Ph.D. degree from Texas A&M University, College Station, TX, USA, in 2000, all in electrical engineering.

He is the Canada Excellence Research Chair Laureate with McMaster University, Hamilton, ON, Canada. He is also the holder of the NSERC/Stellantis Industrial Research Chair in Electrified Powertrains and Tier I Canada Research Chair in Transportation Electrification and Smart Mobility. Before joining McMaster University, he was the Harris Perlstein Endowed Chair Professor of engineering and the Director of Electric Power and Power Electronics Center and Grainger Laboratories, Illinois Institute of Technology, Chicago, IL, USA. He was the founding Editor-in-Chief for the IEEE TRANSACTIONS ON TRANSPORTATION ELECTRIFICATION from 2014 to 2020.

Tobias Geyer's photograph and biography not available at the time of publication.

Ralph Kennel's photograph and biography not available at the time of publication.

Tomislav Dragicevic's photograph and biography not available at the time of publication.

Davood Arab Khaburi's photograph and biography not available at the time of publication.

Zhen Zhang's photograph and biography not available at the time of publication.

Mohamed Abdelrahem's photograph and biography not available at the time of publication.

Nenad Mijatovic's photograph and biography not available at the time of